Osteoarthritis and Cartilage Biotribology

Ren, Ke

DOI:
10.33612/diss.258884793

CHAPTER 4

Dopamine-conjugated hyaluronic acid delivered via intra-articular injection provides articular cartilage lubrication and protection

This contents of this chapter are based on:
***Ren K**, Wan H, Kaper HJ, Sharma PK (2022) Dopamine-conjugated hyaluronic acid delivered via intra-articular injection provides articular cartilage lubrication and protection. J Colloid Interface Sci 619:207–218. doi: 10.1016/j.jcis.2022.03.119*

Abstract

Due to its high molecular weight and viscosity, hyaluronic acid (HA) is widely used for viscosupplementation to provide joint pain relief in osteoarthritis. However, this benefit is temporary due to poor adhesion of HA on articular surfaces. In this study, we therefore conjugated HA with dopamine to form HADN, which made the HA adhesive while retaining its viscosity enhancement capacity. We hypothesized that HADN could enhance cartilage lubrication through adsorption onto the exposed collagen type II network and repair the lamina splendens. HADN was synthesized by carbodiimide chemistry between hyaluronic acid and dopamine. Analysis of Magnetic Resonance (NMR) and Ultraviolet spectrophotometry (Uv-vis) showed that HADN was successfully synthesized. Adsorption of HADN on collagen was demonstrated using Quartz crystal microbalance with dissipation (QCM-D). *Ex vivo* tribological tests including measurement of coefficient of friction (COF), dynamic creep, in stance (40 N) and swing (4 N) phases of gait cycle indicated adequate protection of cartilage by HADN with higher lubrication compared to HA alone. HADN solution at the cartilage-glass sliding interface not only retains the same viscosity as HA and provides fluid film lubrication, but also ensures better boundary lubrication through adsorption. To confirm the cartilage surface protection of HADN, we visualized cartilage wear using optical coherence tomography (OCT) and atomic force microscopy (AFM).

Keywords: Lubrication, Cartilage, Boundary lubrication, Weeping lubrication, Hyaluronic acid

1. Introduction

Articular cartilage typically provides low friction (Coefficient of friction, $\mu < 0.01$) in healthy hip, knee and other articular joints[1]. The mechanisms of the superlubricity properties of cartilage are still under debate; prevailing theories are based on a combination of fluid film lubrication (**Fig. 1b**) and boundary lubrication (**Fig. 1c**)[2–4]. The fluid film lubrication requires high viscosity of the synovial fluid [5] along with the unique biphasic structure of curved articular cartilage[6]. Due to wedge formation between the curved cartilage surfaces at high sliding speeds, high viscosity and low loads, the hydrodynamic fluid formation could take place as suggested by MacConaill[7]. Besides the hydrodynamic effect, hydrostatic compression of cartilage can also lead to fluid formation as suggested by McCutchen[8], who showed that articular cartilage – being deformable, porous and saturated with fluid – weeps out fluid into the sliding interface upon hydrostatic compression [8,9]. Most of the applied load is initially supported by the fluid film, giving rise to very low friction, but the load is gradually transferred to solid-solid contact due to creep of the cartilage. During this solid-solid contact, boundary lubrication – attributed to the lamina splendens – becomes the predominant lubrication mechanism[9]. Macromolecular complexes of polysaccharides, lipids and glycoproteins – including hyaluronic acid (HA), phospholipids, aggrecan and lubricin – then adsorb. This gives rise to the acellular, lamina splendens layer on the cartilage surface[1,10–13].

A complete gait cycle[9,14] contains regions of high and low loads and sliding velocities in which fluid film, boundary and mixed lubrication mechanisms (i.e. simultaneous fluid film and boundary lubrication) remain active. High viscosity (η) has always been accepted as a necessary property for the synovial fluid to provide fluid film lubrication to the synovial joint[5,14–17]. In addition, surface active macromolecules such as proteoglycan 4 (PRG4, also called lubricin) and surface active phospholipids (SAPL) in combination with HA are deemed necessary to provide boundary lubrication[3,4]. Thus, any attempt to enhance biolubrication in the synovial joints needs to take into consideration both the high viscosity and surface adhesive functionality of the treatment.

Osteoarthritis (OA) is the most prevalent disease of articular joints, affecting around 15% of the population worldwide[18]. The central pathological feature of OA has traditionally been attributed to progressive loss of articular cartilage, which is mainly related to the degradation of extracellular matrix (ECM) and changes in the composition of cartilage and the synovial fluid[2,19]. This progressive loss of articular cartilage is associated with increased friction and wear of the cartilage. To relieve pain during early OA, an intra-articular injection of HA, also

called viscosupplementation, is administered with the aim of enhancing lubrication[20]. The clinical efficacy of a hyaluronan-containing injection compared to placebo is under debate, with multiple studies reporting no benefit[21,22]. After reviewing 63 trials, a Cochran study[23] reported that the effect is visible only after 5-13 weeks following multiple injections, with pain improvement in 11% to 54% of the patients and function improvement in 9 % to 15 %[24,25]. A possible explanation is that exogenous HA only increases the viscosity of the synovial fluid, thus improves the chances of fluid film lubrication. However, previous studies have shown that modified HA adheres or adsorbs to articular cartilage surfaces better than unmodified HA[26–28].

In designing our study, we therefore addressed the following questions. Is it possible to circumvent these adsorption limitations of HA? Is an injectable formulation possible with which exogenous HA adsorbs well onto intraarticular surfaces including cartilage to enhance boundary lubrication [27] and simultaneously enhances viscosity to support fluid film lubrication [15]? As a solution, we proposed using adhesive HA that has been conjugated with 3,4-dihydroxy-L-phenylalanine (Dopamine) via carbodiimide chemistry[29,30]. Dopamine-conjugated hyaluronic acid is an advanced biomaterial that has been widely used in clinical therapy including tissue adhesives[31], anti-biofouling bioelectrodes[32], capturing circulating tumor cells (CTCs)[33], chemophotothermal cancer therapy[34] and modification of Cardiovascular Implanted Devices[35]. However, this molecule has not yet been used in the field of biotribology to lower friction and enhance lubrication. When conjugated with dopamine, HA forms HADN, whose ortho-dihydroxyphenyl (catechol) group acts as an adhesive on various inorganic/organic surfaces [36] under wet conditions. We hypothesized that HADN would give rise to artificial cartilage lubrication enhancement through fluid film and boundary lubrication.

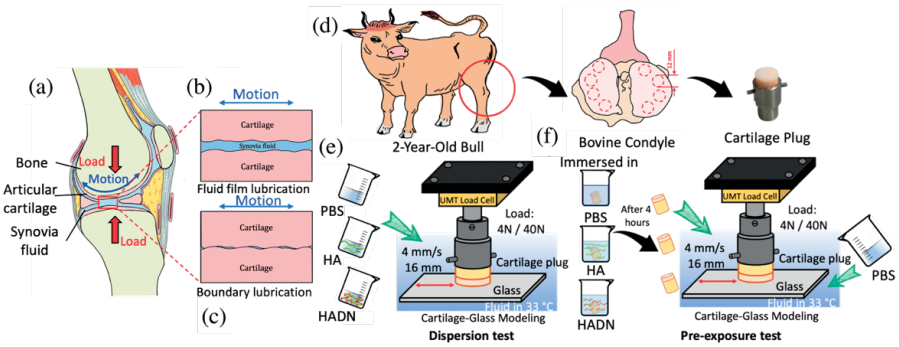

Fig. 1 Schematic of a synovial joint with cartilage lubrication modes and schematic of cartilage tribology measurements. (a) Basic structure of synovial joint. (b) Fluid film lubrication mode and (c) Boundary lubrication mode expected during different phases of the gait cycle. (d) bovine osteochondral plugs were obtained from bovine condyles. (e) Dispersion test, where osteochondral plugs were slid against glass in PBS, HA or HADN solution, respectively. (f) Pre-exposure test, where osteochondral plugs were incubated in PBS, HA and HADN solution, respectively, for 4 hours. The treated plugs were then slid against glass in PBS solution.

2. Materials and Methods

2.1 Synthesis of HADN

Hyaluronic acid (Kraeber & Cogmbh, Germany) with a molecular weight of 600 kDa was coupled to dopamine hydrochloride (CAS no. 62-31-7, certified reference grade material, Sigma-Aldrich) with the help of N-(3-Dimethylaminopropyl)-N-ethylcarbodiimide hydrochloride (EDC, purity≥98.0% (AT), Sigma, CAS no.25952-53-8). Briefly, 50 mg HA was dissolved in 10 ml Phosphate Buffer solution (PBS) at pH 5 adjusted by hydrochloric acid (HCl, CAS no. 7647-01-0, ACS reagent grade, Sigma-Aldrich). Then 15 mg EDC and 20 mg dopamine were added to the HA solution at pH 5 and allowed to react for 5 hours. The reaction was protected with nitrogen. Unreacted chemicals and byproducts were removed by extensive dialysis (molecular weight cut-off: 3500 Da, spectrum medical industries, USA) for 3 days in deionized water (pH 5), which was exchanged every 3 hours (at first 12 hours). Later on the dialysis water was changed every 8 hours. Then conjugate product was lyophilized and stored at 4°C in a moisture-free desiccator for further use.

Nuclear Magnetic Resonance (NMR) and Ultraviolet spectrophotometry (Uv-vis) were used to characterize HADN. A lyophilized sample was dissolved in deuterated water at 5 mg/ml for 1H-NMR (Bruker Avance, 400 MHz) analyses. Dopamine solutions with various concentrations ranging from 0.1 mM to 1 mM in PBS were prepared and their spectrum absorbance at 280 nm was measured by Uv-Vis spectrum (Beckman, USA) with a cuvette of 1cm wide to make a standard curve by linear fitting. The absorbance at 280 nm of 1 mg/ml HADN was used to calculate the conjugation degree by comparing it with standard curve.

2.2 Viscosity measurement for HA and HADN solutions using a rheometer

HA and HADN solution with 2 mg/ml in 10 mM PBS buffer were prepared for viscosity evaluation by modular compact rheometer (Physica MCR 300, Anton Paar GmbH, Austria) with a plate and plate geometry of a radius of 50 mm (Measure system: PP50). In this study, steady-shear viscosity as a function of shear rate from 0.01 s^{-1} to 100 s^{-1} was evaluated. Both samples were tested at least 3 times, during which 2 ml solution was used in single experiment for a period of 120 s. To ensure the fresh status of the solutions we used during the experiments, the HA and HADN solutions were freshly prepared before each experiment.

2.3 HADN adsorption on collagen type II using quartz crystal microbalance with dissipation (QCM-D)

Molecular adsorption on gold coated, AT-cut quartz crystal sensor discs was monitored through QCM-D in terms of frequency (Δf) and dissipation (ΔD) shifts. Higher negative frequency shift ($-\Delta f$) means higher adsorbed mass while higher dissipation (ΔD) means more viscous, fluffy or hydrated adsorbed mass[37].

The disc-shaped, gold coated, AT-cut quartz QCM sensors were cleaned thoroughly by rinsing with ultrapure water (Milli-Q water), dried with N_2, exposed to UV/ozone for 10 min, and then immersed in a 3:1:1 mixture of ultrapure water, ammonia solution (NH_3), and hydrogen peroxide (H_2O_2) at 70−80 °C for 10 min. After that, the gold crystals were rinsed with Milli-Q water, dried by N_2 and treated with UV/ozone for another 10 min. Inside the QCM-D ((Q-Sense E4, Västra Frölunda, Sweden), 10 mM phosphate-buffered saline (PBS) was allowed to flow through the chamber and passed over the crystals using a peristaltic pump for creating a baseline for the measurements. For this and all other QCM-D measurements, a flow rate of 50 µl/min at 22 °C was used.

The QCM sensors were first coated with a layer of collagen type II, using a protocol described elsewhere [38]. In short, 2 mg/ml of collagen type II in 0.5 M acetic acid was diluted 50 times with ultrapure water (Milli-Q water) to form a concentration of 40 μg/ml in 10 mM acetic acid. To converting the molecules to fibrils, 10 min before flowing into the QCM-D, 66% v/v of 250 mM phosphate-buffered saline was added to the solution, resulting in a pH of 7.3. The collagen type II coating was formed through the following steps: (1) 10 mM PBS was streamed through the chamber and over the crystal for a baseline; (2) 250 mM phosphate-buffered saline was streamed through this chamber; (3) the collagen type II fibril solution was streamed over the crystal to adsorb. Since the adsorption of collagen type II did not reach a plateau by itself, the flow of the solution was stopped after achieving the desired adsorption ($-\Delta f \sim 300$ Hz), which would ensure complete coverage of the gold-coated QCM crystal surface. This was followed by a rinse with 250 mM phosphate-buffered saline (4); this was followed by a rinse with 10 mM PBS to remove the dissociative collagen molecules and obtain the collagen type II layer in physiological state (5). Using the frequency and dissipation shift values and the QSoft program from Q-Sense, we estimated the collagen type II layer to be 158.90 nm $\pm$ 6.80 nm (n = 3) thick. Collagen type II was obtained from adult human articular cartilage (stock concentration of 2 mg/ml in 0.5 M acetic acid) and was isolated as described previously [39]. Once the QCM crystal was coated with collagen type II, (6) HA or HADN dissolved in 10 mM PBS at 2 mg/mL was allowed to adsorb for 1 hour followed by (7) a thorough rinsing with 10 mM PBS [13].

2.4 Lubrication provided by HA and HADN to cartilage against glass

2.4.1 Preparation of osteochondral plug

Fresh bovine knee joints (from bulls approximately two-years old) were obtained from a local abattoir (Kroon Vlees b.v., Groningen, the Netherlands) and dissected 24 hours after slaughter. The joints were opened at room temperature (20-24°C), and any joints with visible cartilage redness or damage were excluded. Cartilage plug samples with a diameter of 12 mm were drilled from the central area of both femoral condyles using hollow drill bits (**Fig. 1d**). Drilling and cutting was performed under continuous wetting and cooling with PBS buffer. Extreme care was taken not to touch the cartilage surface at any time during the plug preparation. Osteochondral plugs were stored in PBS at 4 °C before tribological experiments and used within 24 h.

2.4.2 Tribology test

The tribology tests were performed using UMT-3 (Universal Mechanical Tester, Bruker Corporation, USA) in a pin-on-plate reciprocating sliding configuration. The osteochondral plug was mounted under the load cell and slid against borosilicate glass mounted on a moving stage (**Fig. 1e & f**). Both HA and HADN were tested in two ways. To mimic the joint injection environment in Test 1 (the 'Dispersion' tribological-test), the osteochondral and glass were kept continuously submerged in PBS buffer containing HA (2 mg/ml) or HADN (2 mg/ml) solutions at 33°C during sliding (**Fig. 1e**). In Test 2 (the 'Pre-exposure' tribological test), the osteochondral plugs were pre-exposed to PBS buffer, HA (2 mg/ml in PBS) or HADN (2 mg/ml in PBS) solutions at 33°C for 4 hours (**Fig. 1f**). After that, the plugs were carefully rinsed with PBS and mounted on the UMT-3 and slid against glass submerged in PBS at 33 °C. To mimic the swing and stance phase of the gait cycle, in both the dispersion test and pre-exposure test a load of 4 N (swing phase) and 40 N (stance phase) was applied separately, resulting in an average contact pressure of 0.4 and 1 MPa, respectively [40]. In both the dispersion test and pre-exposure test, a sliding velocity of 4 mm/s was used over a sliding distance of 16 mm for 1 hour both, resulting in 450 cycles during each tribological test.

Average dynamic COF and dynamic creep were measured. For presentation of results (**Fig. 4**, **6**) an average dynamic COF was obtained by calculating the mean level of COF (friction force/normal force) in each cycle. To simplify the display even further, average COF was then calculated for every 50-cycle interval until 450 cycles (i.e. cycle 0, cycle 50, cycle 100 and so on). Dynamic creep was obtained by recording the cartilage deformation using the z-position of the carriage at the start of each cycle during reciprocating sliding. These values were recorded for every 50-cycle interval until 450 cycles.

2.5 Visualization of cartilage wear after tribology test

2.5.1 Optical coherence tomography (OCT) measurement

Immediately after sliding during the dispersion test and pre-exposure test, bovine cartilage plugs with and without rubbing tests were put on the OCT table for cross-section wear visualization. Samples were measured using OCT Ganymede II (Thorlabs Ganymede, Newton, NJ, USA) with a 930 nm center wavelength white light beam and a Thorlabs LSM03 objective scan lens, which can provide a maximum scan area of 100 mm^2. 2D images had a fixed size of 5000 pixels with pixel size varying with magnification in the horizontal (x-y) direction while containing a variable number of pixels with 2.68 µm/pixel in the vertical (z) direction. The scan area was 7.68 × 2.74 mm^2. Images were created by the OCT software (ThorImage

OCT 4.1) using 32-bit data.

2.5.2 Atomic Force Microscopy

After OCT, the osteochondral plugs were fixated with paraformaldehyde (Sigma, CAS no. 30525-89-4) for 45 min at room temperature, followed by rinsing with PBS. The cartilage surface roughness was measured by an atomic force microscope (AFM) (Nanoscope IV Dimensiontm 3100, USA) equipped with a dimension hybrid XYZ SPM scanner head (Veeco, New York, USA) with a scan area of 30 × 30 μm^2 and a scanning frequency of 1 Hz, with a scanning resolution (512 × 512 pixels). The surface topography was measured by AFM operating with the contact mode in air using a non-conductive silicon nitride probe (DNP-10, Bruker Corporation, USA) at a constant normal force of 5 nN. Data analysis was performed on NanoScoop Analysis (also Bruker). The root mean squared roughness (RMS) $R_q = \sqrt{\frac{1}{n}\sum_{i=1}^{n} y_i^2}$ was calculated from the average height at 3 locations per sample [41]. Due to the sample curvature, all images were flattened with 1st or 2nd order before calculating the roughness.

2.5 Statistical Analysis

All data are expressed as means ± SD, calculated from three independent experiments. Statistical analysis was performed with GraphPad Prism version 8.0 (GraphPad Software, La Joola California, USA). Significant differences between groups was determined by using two-tailed Student's t-test analysis in viscosity tests and QCM-D measurements and one-way ANOVA analysis in tribology tests. Significance was defined as $p < 0.05$.

3. Results and discussion

3.1 Dopamine conjugation with hyaluronic acid: HADN synthesis and its characterization

HADN was prepared by carbodiimide chemistry with N-(3-Dimethylaminopropyl)-N-ethylcarbodiimide hydrochloride (EDC) coupling reaction[29,36,42,43]. A schematic representation of synthetic procedure is shown in **Fig. 2a**. The multiple peaks observed between δ = 6.7 ppm and δ = 7.0 ppm in 1H-NMR spectra shown in **Fig. 2b** are associated with protons of the aromatic ring[30]. Chemical shift at 2.03 ppm is associated with protons of N-$COCH_3$ [30] demonstrating that HADN conjugation was successful. The results also were

confirmed by Uv-visible spectrophotometer in **Fig. 3c**. An absorbance band around 280 nm, the characteristic absorbance of catechol, was observed in HADN while not shown in HA alone. Dopamine solutions with different concentrations from 0.1 mM to 1 mM in PBS were prepared. Their spectrum absorbance at 280 nm was measured by Uv-Vis spectrum. Then the standard curve was calculated by linear fitting in **Fig. S1**. Based on a standard curve and the A280 nm of the synthesized product, the conjugation was calculated as about 22%. This means that on average, every fifth carboxyl is conjugated with DN. Amidation by a carbodiimide coupling method[30] is widely used in biomaterial applications due to its features of highly effective and reproducible. Different equivalent proportion can yield different conjugation degree. In the present study, we chose a 22% conjugation because less than 10% is conventionally considered to be a low catechol conjugation level for polymer. Likewise, a conjugation degree of over 30 % is regarded as a high catechol conjugation for polymer[44,45].

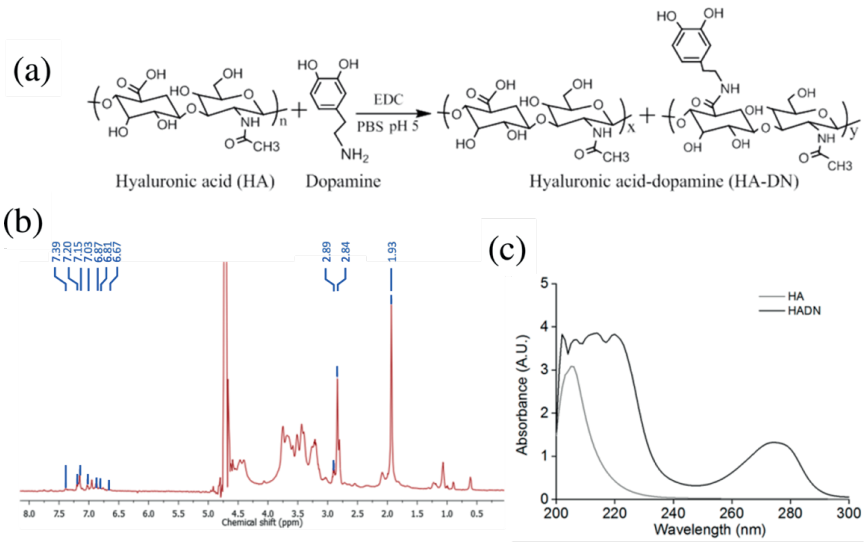

Fig. 2 (a) The schematic representation of the procedure to synthesize HADN. (b) The H-NMR spectrum of HADN. (c) UV-Vis spectra of the conjugate (HADN) and the control (HA).

3.2 Viscosity comparison between HA and HADN

The viscosities of the HA and HADN solutions (2 mg/ml in PBS buffer) are shown in **Fig 3a**. Both HA and HADN samples generally displayed characteristic shear-thinning behavior

reflected in a reduction in viscosity with increasing shear rate [46]. In the HADN solution, the viscosity went up to a peak of 0.570 Pa s ± 0.451 Pa s at shear rate of 0.025 s^{-1} but dropped sharply to about 0.004 Pa s at 10 s^{-1}. The viscosity of HADN stabilized at 0.004 Pa s until 100 s^{-1}. In contrast, HA solution had the highest viscosity value (0.232 Pa s ± 0.095 Pa s) at a shear rate of 0.040 s^{-1}, which then decreased to 0.003 Pa s, but this didn't change until a shear rate of 100 s^{-1} was reached. No significant difference was found between HADN and HA viscosity at any shear rate, which means that HADN solution with a concentration of 2 mg/ml in PBS buffer has similar viscosity behavior as the HA solution.

3.3 HADN adsorption onto collagen type II

The Δf and ΔD time plots for the adsorption of collagen type II followed by HADN or HA are shown in **Fig. 3b, c & d**, where **Fig. 3c** represents the period during which HADN or HA adsorbed alone. Collagen type II adsorbed very well onto the gold-coated QCM crystal: a Δf of −285.08 ± 0.13 Hz was measured after rinsing with 10 mM PBS buffer. The -ΔD/Δf value was 85.47 ± 5.63 × 10^{-6}, which indicates a highly viscoelastic layer.

In our experimental design, this collagen type II layer represented the exposed collagen fibers due to the removal of the lamina splendens. HA showed barely any adsorption onto collagen type II with a frequency shift of -3.64 ± 2.07 Hz after 60 min of flow. In contrast, HADN readily adsorbed onto collagen type II with a Δf of -25.00 Hz ± 5.35 Hz. HADN was not washed off during the final PBS rinsing step, thus indicating irreversible adsorption (**Fig. 3c**). The viscoelasticity of the HADN or HA layer on collagen type II was evident from the ratio of dissipation to frequency shift (-ΔD/Δf × 10^{-6}), as shown in Table 1. The viscoelasticity of the HADN layer on collagen type II was much higher than that of HA, with a value of 0.42 ± 0.18 compared to 0.09 ± 0.07 for HA.

This demonstrates a clear affinity of HADN for collagen type II through electrostatic interactions under physiological pH and ionic strength[47] and an inability of HA to adsorb onto collagen type II.

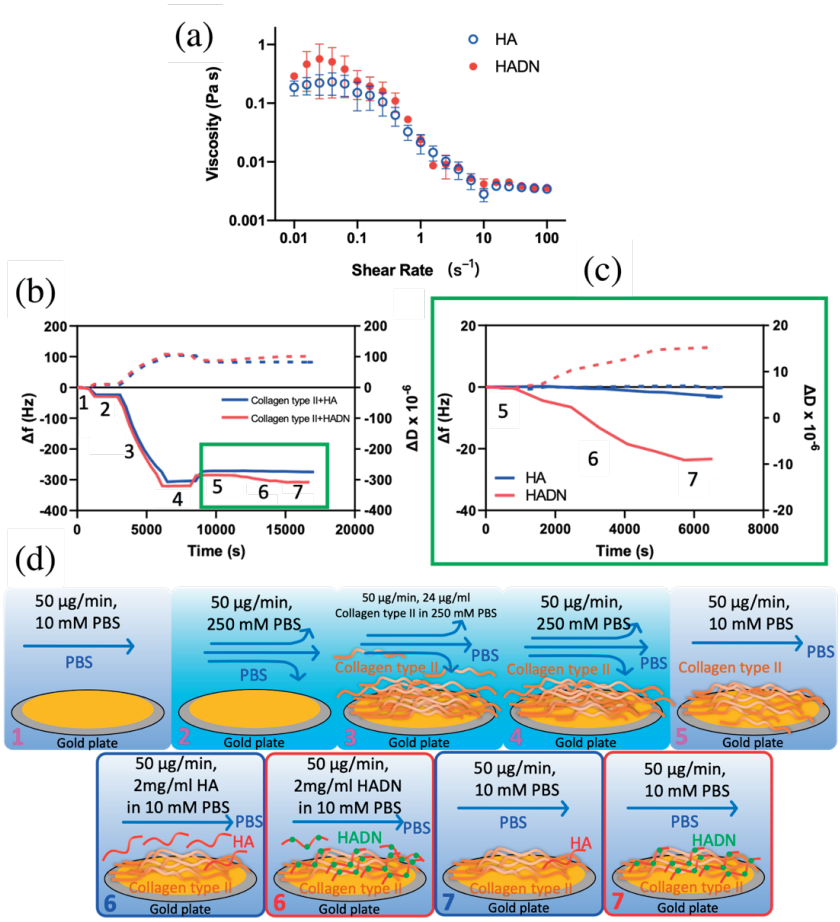

Fig. 3 (a) Viscosity of 2 mg/ml HA and HADN in PBS under a shear rate ranging from 0.01 to 100 s^{-1}. Error bars represent the standard deviation across three independent measurements. The kinetics of HADN and HA adsorption on the collagen type II layer measured with QCM-D are also shown, in which solid lines represent frequency shift (Δf) and dotted lines represent dissipation (ΔD × 10−6). (b) Adsorption of collagen type II followed by HA and HADN adsorption. (c) HADN and HA adsorption processes. Steps 1 to 7 are explained in the text and pictorially in D. (d) Schematic of steps followed during collagen type II experiment followed by HADN and HA adsorption.

Table 1 The frequency shift (-Δf, indicating adsorbed mass) and the ratio of dissipation to frequency shift (-

$\Delta D/\Delta f \times 10^{-6}$) indicating the fluffiness and viscoelasticity of the layer after adsorption of HA and HADN onto the collagen type II layer. Error bars represent the standard deviation across three independent measurements, *p < 0.05: compared with the HA samples.

Substrate	$-\Delta f$ (Hz)		$-\Delta D/\Delta f \times 10^{-6}$ (s)	
	HA	HADN	HA	HADN
Collagen-type II	3.64 ± 2.07	25.00 ± 9.35 *	0.09 ± 0.07	0.42 ± 0.18 *

3.4 *Ex-vivo* lubrication provided by HA and HADN to cartilage as compared to PBS

3.4.1 Dispersion tribological test

During the dispersion tests, the effects of viscosity enhancement and adsorption of HA and HADN on the friction and wear of cartilage were observed. **Fig. 4** shows the COF (**Fig. 4a**) and dynamic creep (**Fig. 4b**) for osteochondral plugs sliding against glass at 4 N and 40 N. The COF at 4 N was higher than that of 40 N. At both loads, the COF of cartilage samples submerged in PBS was the highest: 0.51 ± 0.04 in the swing phase (4 N) and 0.258 ± 0.03 in the stance phase (40 N) at cycle 450. Compared to PBS, the samples submerged in HA solution had a significantly lower COF: 0.37 ± 0.02 at 4 N and 0.20 ± 0.01 at 40 N. Samples submerged in HADN solution showed a further decrease in COF: 0.33 ± 0.06 the in swing phase (4 N) and 0.17 ± 0.01 in the stance phase (40 N). These values were significantly lower than the values measured in the presence of PBS. The average COF in the presence of HADN was always lower than in the presence of HA at both the loads, but this difference was not statistically significant. The results indicate that HADN efficiently lubricated the cartilage against glass during both the swing and stance phase.

Dynamic creep was higher at 40 N (~1MPa) than at 4 N (~0.4 MPa) due to higher weeping of fluid and depressurization of the cartilage[8,48]. At the end of 450 cycles the creep at 4 N was 0.08 mm ± 0.03 mm in the PBS group, 0.14 mm ± 0.03 mm in the HA group and 0.16 mm ± 0.04 mm in the HADN group. At 40 N, the creep was 0.41 mm ± 0.05 mm in the PBS group, 0.37 mm ± 0.02 mm in the HA group and 0.38 mm ± 0.03 mm in the HADN group. The lubricant used did not make any significant difference in the amount of creep at both loads. This dynamic creep was the effect of depressurization of the cartilage due to release of

interstitial fluid, as reported by Ateshian et al.[49,50].

The roughness of the cartilage surface (**Fig. 4c**) can change due to wear at the surface. We therefore measured the roughness of bovine cartilage after tribology. Osteochondral sliding against glass, at 4 N while, submerged in HADN showed a roughness measured on AFM of 133 nm ± 4 nm, which was closest to intact cartilage (control) with roughness of 134 nm ± 7 nm. In comparison, sliding in presence of PBS and HA caused an insignificant increase in roughness i.e., 189 nm ± 25 nm and 260 nm ± 95 nm respectively. At 40 N, the osteochondral plug that was submerged in HADN showed a roughness of 169 nm ± 42 nm, which was also closest to intact cartilage. However, sliding in the presence of PBS caused a significant increase in roughness (245 nm ± 17 nm), while sliding in the presence of HA caused an insignificant increase (191 nm ± 19 nm).

After tribology measurements, cartilage surface morphology was displayed in the surface view of AFM, and the cartilage subsurface structure was examined by OCT (**Fig. 5**). AFM or OCT results both indicated a clear advantage of the wear-protection of HADN solution during tribological experiments. In the image of native cartilage without rubbing (group control) in **Fig 5a**, the surface was flat and intact due to an uneven and amorphous protein layer. This layer could have been the lamina splendens composed of various biomacromolecules on top of collagen network[38]. After rubbing with a low load (4N) in the swing phase, the cartilage submerged in PBS, HA and HADN solution had damage on the surface, as shown in **Fig. 5a**. More specifically, there were some bigger spalls on the surface of PBS group and many smaller scratches on the surface of HA samples (red arrows) compared with a smooth surface for the HADN group. The higher friction force observed on surface of cartilage submerged in PBS and HA resulted in severe damage to superficial layer and exposure of collagen fibers [47]. Due to weeping lubrication, much more fluid reached the sliding interface, which formed thicker fluid film between cartilage and glass and resulted in lower friction at 40 N. Consequently the abrasion condition of all rubbing cartilage was lighter. Moreover, the surface of osteochondral plugs that were submerged in HADN were most similar to intact cartilage (control group) in the OCT result (**Fig. 5b**). In contrast, obvious damage (yellow arrows) with a rougher surface was induced at 4 N and 40 N on the surface of cartilage submerged in PBS. Osteochondral plugs submerged in HA also showed a slightly rougher surface, but less severe. In summary, HADN solution as an intraarticular injection not only provides better lubrication (lower friction) but also lower cartilage wear as measured by roughness.

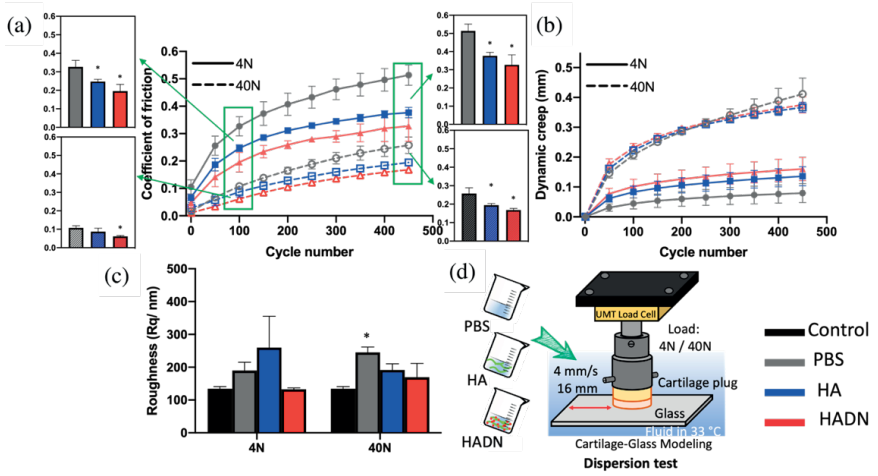

Fig. 4 Tribological performance of cartilage-glass interface in PBS, HA and HADN solutions at low load (4 N) and high load (40N) in dispersion test. (a) The time-depended dynamic COF of cartilage rubbing against glass in different solutions. (b) The dynamic creep of different cartilage samples during friction measurement. (c) The surface roughness of cartilage after rubbing in different solutions. (d) Schematic of tribology measurements of liquid tribological test setup. Error bars represent the standard deviation across three independent measurements, *p < 0.05: compared with the PBS samples in **Fig. a**; compared with the control samples in **Fig. c**.

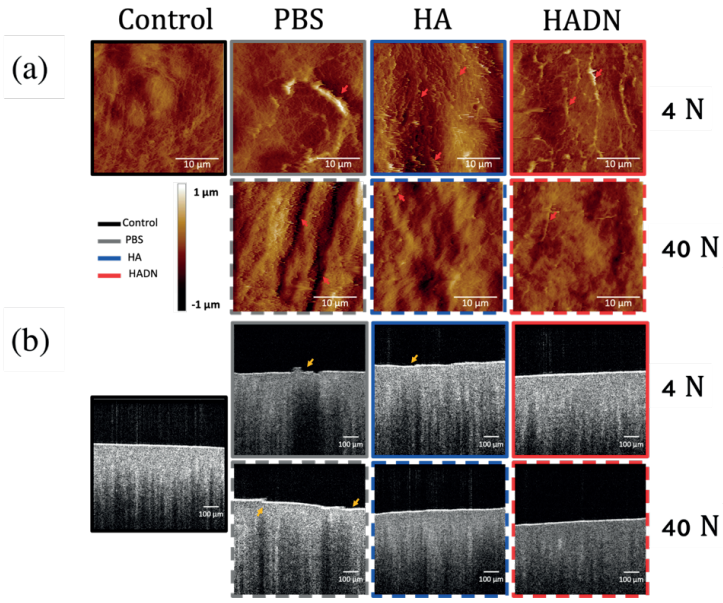

Fig. 5 (a) Surface morphology of cartilage surface measured by AFM with a scan area of 30×30 μm^2. Red arrows show the damage resulted from rubbing. (b) Lateral view of the cartilage cross-section using OCT after rubbing against glass in different solutions in dispersion test. Yellow arrows show the damage due to wear after tribological test.

3.3.2 Pre-exposure tribological test

Pre-exposure tests were performed to study the effect of adsorbed HA and HADN only on cartilage wear and friction (**Fig. 6 & 7**). The COF (**Fig. 6a**) of cartilage samples submerged in PBS was the highest of the three groups: 0.51 ± 0.04 in the swing phase (4N) and 0.258 ± 0.03 in the stance phase (40N) at cycle 450 (**Fig. 6a**). Compared to PBS, at 4 N samples pretreated with HA solution showed reduced COF of 0.41 ± 0.06, but the difference was not significant. However, for cartilage pretreated with HADN solution, a significantly lower value of 0.31 ± 0.02 was measured. At 40 N, the COF value of HA sample (0.22 ± 0.03) was very similar to that of PBS. A significantly lower value of 0.18 ± 0.01 was also observed in the stance phase (40 N) for cartilage pretreated with HADN. Clearly, HADN that is absorbed onto the cartilage surface provides better lubrication at the cartilage-glass interface submerged in PBS during both swing and stance phases.

Dynamic creep (**Fig. 6b**) showed similar trends in the pre-exposure test and the dispersion tribological test. Irrespective of the pre-exposure fluid, dynamic creep was higher at 40 N than at 4 N[8]. After 450 cycles, the observed creep at 4 N was 0.10 mm ± 0.03 mm in the PBS group, 0.16 mm ± 0.01 mm in the HA group and 0.18 mm ± 0.07 mm in the HADN group, but at 40 N it rose to 0.47 mm ± 0.03 mm in the PBS group, 0.35 mm ± 0.05 mm in the HA group and 0.30 mm ± 0.13 mm in the HADN group.

After 450 cycles of sliding, the roughness (**Fig. 6c**) of osteochondral plugs pretreated with PBS was 315 nm ± 90 nm at 4 N and 251 nm ± 424 nm at 40 N, which was significantly higher than 134 nm ± 7 nm observed for intact cartilage. After HADN pretreatment, the roughness of the cartilage was very similar to intact cartilage: 171 nm ± 40 nm at 4 N and 145 nm ± 3 nm at 40 N. Osteochondral plugs pretreated with HA had a roughness of 178 nm ± 97 nm during the swing phase (4 N), and 160 nm± 3 nm during the stance phase (40 N).

Fig. 7 shows the surface morphology after sliding. As shown in **Fig. 7a** (AFM images), damage was much less frequent and less severe at both 4 N and 40 N in the osteochondral plug that was pretreated with HADN. In contrast, HA and PBS pretreatment did not provide resistance to the friction force on the cartilage surface, on which more damage and wear (red arrows) was visible. OCT cross-section view images (**Fig. 7b**) showed damage on the entire osteochondral surface at both loads. Cartilage pretreated with HADN solution had a surface with some small hills (yellow arrows) during the swing phase (4 N) and stance phase (40 N). In contrast, at 4 N larger and deeper damaged areas appeared on the surfaces that were pretreated with HA, while at 40 N, the damage was less severe. Osteochondral plugs that were pretreated with PBS showed a slightly rougher surface compared to HA pretreated samples at both loads (4 N and 40 N). Therefore, HADN pretreatment showed a tendency not only to reduce the COF, but also appeared to prevent wear and damage at both loads.

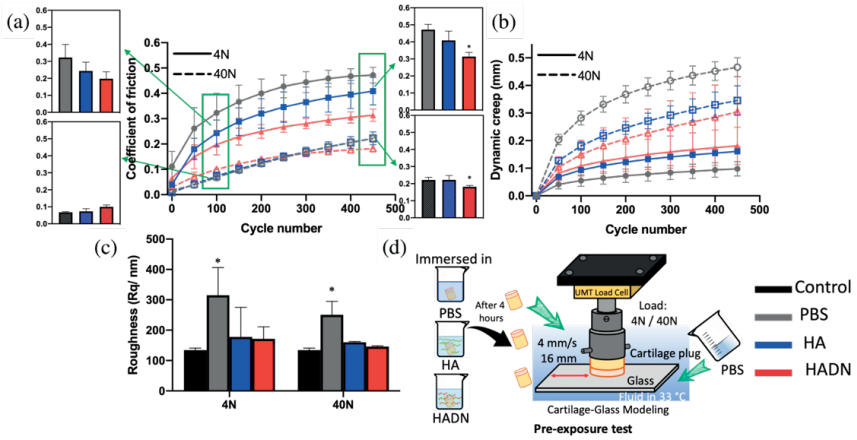

Fig. 6 Tribological performance of cartilage-glass interface in PBS at low load (4 N) and high load (40N) in pre-exposure test. Before the test, cartilage samples were incubated separately in PBS, HA and HADN solution for 4 hours. (a) The time-dependent dynamic COF of cartilage rubbing against glass (b) The dynamic creep of various cartilage samples during friction measurement. (c) The surface contact area of various cartilage samples after rubbing. (d) Schematic of tribology measurements from the pre-incubated tribological test. Error bars represent the standard deviation across three independent measurements, *$p < 0.05$: compared with the PBS samples in **Fig. a**; compared with the control samples in and **Fig. c**.

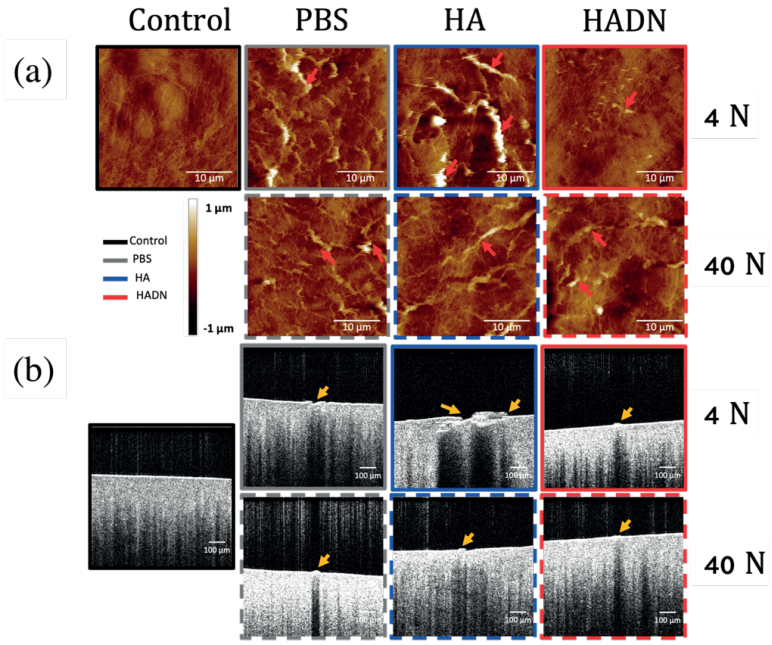

Fig. 7 (a) Surface morphology of cartilage surface measured by AFM with a scan area of 30×30 µm^2, in which red arrows show the damage resulting from rubbing; (b) Lateral view of the cartilage cross-section using OCT after rubbing against glass in various solutions in the pre-exposure test. Yellow arrows show the damage due to wear after the tribological test.

4 Discussion

Dopamine functionalization of HA (HADN) makes it adhesive in nature[36]. Here we investigated whether HADN, when compared to HA, can adhere more effectively to the cartilage surface and enhance lubrication. We used QCM-D to compare the adsorption of HADN and HA on collagen type II, and we performed cartilage-glass reciprocating sliding when HADN was either in dispersion or when cartilage was pre-exposed to HADN for 4 hours. Both 4 N and 40 N were applied to mimic the swing and stance phases of the gait cycle[40].

At both 4 N and 40 N, the general trend for COF evolution during the tribological tests was low COF at the start, but continuously increasing with sliding time (**Fig. 4a & 6b**). This was also shown in previous studies[9,40,51–53]. This increase in COF was accompanied by a

continuous increase in creep (**Fig. 4b & 6c**). This phenomenon was explained by Ateshian et al.[49,50] based on equation 1.

$$\frac{\mu_{eff}}{\mu_{eq}} = 1 - (1 - \varphi)\frac{W^p}{W} \quad (1)$$

Where φ represents the fraction of solid-solid contact area. 1-φ is the contact through the wept out water[54], which is around 0.91 for normal bovine cartilage [54] at the beginning. W^p/W is defined as interstitial fluid load support. μ_{eff} and μ_{eq} are the time-dependent and equilibrium coefficients of friction, respectively.

Our results showed that cartilage was initially compressed quickly (see dynamic creep result from **Fig. 4b & 6b**), resulting in interstitial fluid flowing out from the tissue in sufficient amounts to produce low COF values. But as time passed, more and more fluid was pressed out of the cartilage, resulting in increased solid-solid contact at the cartilage-glass interface, thus leading to an increase in COF.

During the dispersion and pre-exposure tests the cartilage-glass COF at low loads (4 N – corresponding with the swing phase of the gait cycle) was always higher than that at 40 N (corresponding with the stance phase). Previous studies also have shown that the COF decreases with increasing contact force[9,40,53,55]. When compressed at 40 N, much more interstitial fluid from the cartilage weeps out of the pores and merges with the solution (PBS, HA or HADN) to create a thicker fluid film at the cartilage-glass interface. These two observations strongly indicate that hydrostatic fluid weeping and fluid film formation is a predominant cartilage lubrication mechanism.

At the end of the dispersion test, lower friction and wear was observed with both HA and HADN as compared to PBS at both the stance (40 N) and swing phase (4 N) of the gait cycle (**Fig. 4 & 5**). Since the viscosity of both HA and HADN (2 mg/ml) is higher than PBS (1 mPa s), we expected that the hydrodynamic fluid film and boundary lubrication would be active on top of the hydrostatic weeping and fluid film lubrication. However, it was unclear whether hydrodynamic fluid film or boundary lubrication was the dominant mechanism. We therefore performed pre-exposure tribological tests, where the hydrodynamic fluid film contribution to lubrication would be very low due to absence of HA or HADN fluid and the very low viscosity of PBS. At both loads, cartilage pre-exposed to HADN had a significantly lower COF compared to PBS group, while the COF of cartilage pre-incubated in HA approached that of

the PBS group (**Fig. 6**). Similarly, the cartilage surface pre-exposed to HADN appeared to be much more intact compared to cartilage pre-exposed to HA or PBS (**Fig. 7**). The HADN solution clearly enhances cartilage lubrication better than HA. This is probably because HADN molecules not only enhance viscosity to the same level as in the HA solution (**Fig. 3a**), but also because the HADN adsorbs onto the bovine cartilage surface, (**Fig 3b, c & d**, Table 1), thus giving rise to improved boundary lubrication.

Fig. 8 shows a likely explanation of why HADN performs better than HA during cartilage lubrication. In **Fig. 8a & 8b**, the outside fluid is shown as red arrows representing either PBS, HA solution or HADN solution. This fluid is able to flow into the cartilage-glass interface. At an early stage of rubbing (for example, 100 cycles at 4 N and 40 N, **Fig. 8b**), the interstitial fluid due to weeping (the blue arrows in **Fig. 8b**) joins the outside fluid to lubricate the intra-asperity spaces. With continued sliding, the outflow of interstitial fluid decreases considerably, resulting in the disappearance of the intra-asperity spaces. Initially (0 to 100 cycles), a hydrodynamic fluid film with weeping lubrication dominates. Due to higher viscosity of the flowing HA and HADN (hydrodynamic lubrication), during the dispersion test the HA and HADN groups had a significantly lower COF compared to the PBS group (**Fig. 8c** cycle 100 at 4 N and 40 N). During the pre-exposure test, however, no significant difference in COF was found between the three groups due to the absence of flowing HA and HADN molecules (**Fig. 8c** cycle 100 at 4 N and 40 N). In both the dispersion test and pre-exposure test, after around 100 cycles (100 to 450 cycles) boundary lubrication appears to play a more important role than fluid film lubrication **(Fig. 8b**, cycle 450 at 40 N and 4 N). This is probably because numerous bound HADN chains on the cartilage surface are more efficient in immobilizing bound water (**Fig. 9**, Boundary lubrication in both tests), resulting in lower COF in the HADN group (**Fig. 8c** cycle 450 at 40 N and 4 N in both tests). Thus HADN enhances both fluid film lubrication and boundary lubrication, ultimately resulting in a lower COF and protection against cartilage wear.

The biological activity of HA as a lubricant is enhanced when it is conjugated with dopamine (HADN) by becoming more adhesive. Furthermore, HADN has the same viscosity profile as HA, so the fluid film lubrication remains similar to HA. This adhesive nature clearly causes HADN to adsorb onto the cartilage surface, whereas HA does not. This gives rise to higher water-holding capacity at the cartilage surface, resulting in enhanced boundary lubrication. This boundary lubrication enhancement manifests itself not only as low COF, but more importantly as protection against cartilage wear.

In future studies mixtures of HA and HADN could be tested; HADN would preferably adsorb onto the cartilage surface, and a minimum amount of HADN would ensure that the viscosupplementation injections also provide cartilage surface protection.

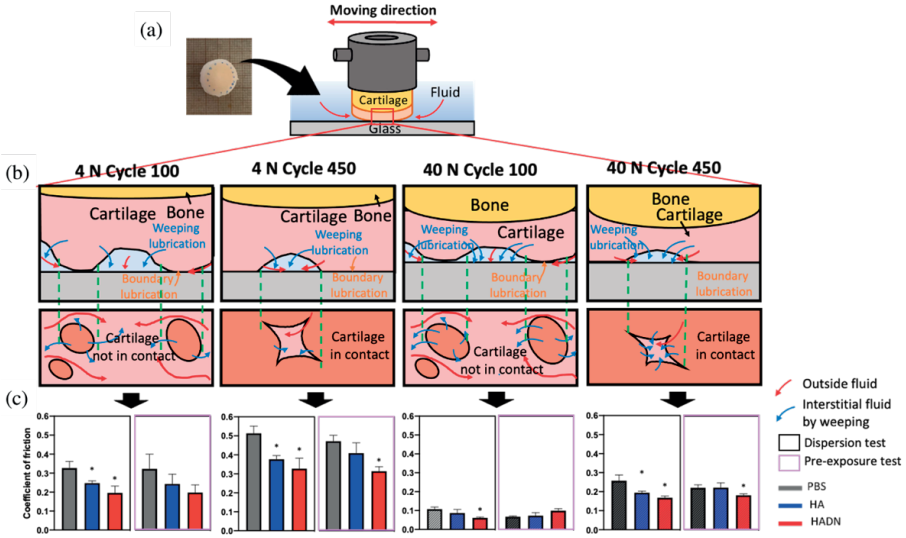

Fig. 8. Schematic illustration at macroscale suggesting the mechanism by which HA and HADN lubricate the cartilage while sliding against glass. (a) Cartilage-glass model. As the illustration of the contact area shows, the outside fluid (shown as red arrows), which represents PBS, HA solution or HADN solution, can flow into the interface between cartilage and glass while the cartilage is rubbing against the glass. (b) Cartilage-glass contact zone. The model is taken from [1]. Initially (at cycle 100), the interstitial fluid due to weeping (shown as blue arrows) and outside fluid (shown as red arrows) flow into small gaps between cartilage and glass. More weeping occurs at 40 N. While sliding, creep increases as fluid flows out of cartilage, resulting in more and more small gaps disappearing; the cartilage begins to contact the glass directly (cycle 450 at 4 N and 40 N) [2]. In this case boundary lubrication dominates. (c) The COF of two tests at cycle 100 and 450.

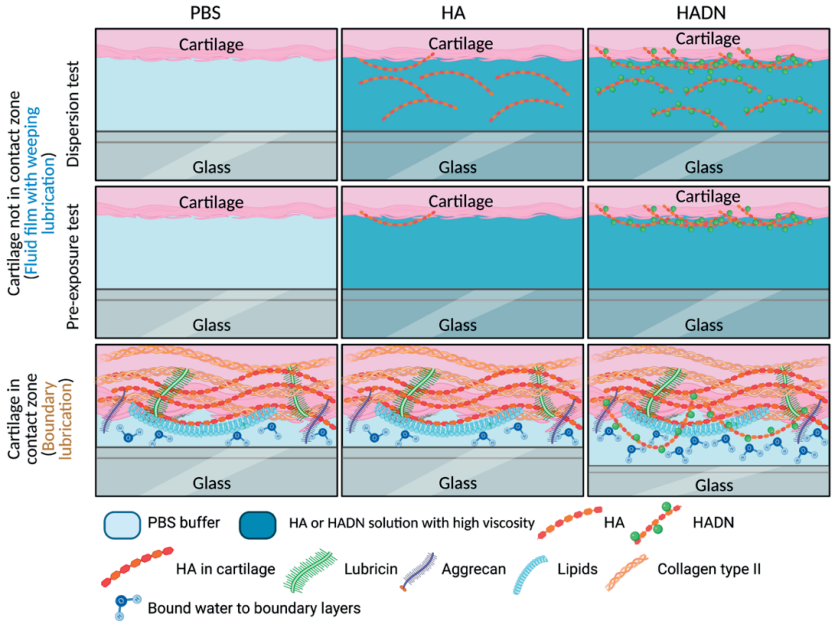

Fig 9. Schematic illustration at microscale suggesting the mechanism by which HA and HADN lubricate the cartilage while sliding against glass. It shows the fate of small gaps at cartilage-glass interface in **Fig. 8b**. Due to the higher viscosity of flowing HA and HADN in the dispersion test, the HA and HADN groups had significantly lower COF compared to the PBS group in the fluid film lubrication condition. In the exposure test, however, no floating HA and HADN was present; the lubricant condition was therefore the same as in the PBS and HA groups, which explains why there was no significant difference in the COF of these two groups. In the boundary lubrication condition, HADN is more efficient in immobilizing bound water on the cartilage surface, resulting in a lower COF.

5. Limitations

In the research presented here, we used a linear reciprocating cartilage-glass model with a constant velocity of 4 mm/s, a sliding distance of 16 mm and two loads of 4 N and 40 N to mimic the knee joint cartilage movement in the human gait cycle. In a real-life situation, however, the velocity and load applied on cartilage change continuously[56]. To avoid this limitation and improve the tribological setup, future research could use dynamic sliding velocity and load corresponding with the natural human gait cycle. Another limitation results

from our choice of glass as a counterface. Cartilage rubbing against cartilage would be a much better simulation of reality than cartilage rubbing against glass. We chose glass as the counterface to ensure valid comparisons with previous research[57] and because it is difficult to obtain large, flat pieces of cartilage to replace glass. In future research, a cartilage condyle against cartilage tibia tribological model could be a better choice on knee joint cartilage lubrication research, if it can be technically realized.

6. Conclusion

In the study, we used hyaluronic acid (HA) conjugated with dopamine (HADN) solution as a novel injectable material for joint cartilage lubrication enhancement. This method improves biolubrication by enhancing both fluid film lubrication and boundary lubrication. It is therefore better than coating biomaterials onto the cartilage surface or using surgical implants, as both of these approaches only improve boundary lubrication. HADN is highly adhesive in nature and readily adsorbs onto the cartilage surface in much higher amounts than unmodified HA. We demonstrated that the fluid film lubrication of HADN was similar to that of HA due to its high viscosity and that HADN also enhanced boundary lubrication due to better adsorption. Moreover, its hydrophilic property ensures that HADN adsorbed onto the cartilage surface can retain water for better boundary lubrication. In our study, this enhanced boundary lubrication reduced cartilage-glass friction and cartilage wear. These findings indicate that injecting HADN together with HA during viscosupplementaion has great potential for lubrication enhancement and chondroprotection. Future *in vitro* or *in vivo* studies are recommended to extend this injectable solution to a different bovine cartilage model including cartilage condyle against cartilage tibia tribological model as well as other tribological body sites, such as artificial hip joints and contact lenses. In addition, to further improve lubrication, corelative biomacromolecules present in cartialge tissue should be conjugated with HADN.

CRediT authorship contribution statement

Ke Ren: Conceptualization, Methodology, Investigation, Data curation, Validation, Formal analysis, Writing – original draft, Writing – review & editing. **Hongping Wan**: Methodology, Data curation, Validation, Formal analysis, Writing – original draft, Writing – review & editing. **Hans J. Kaper**: Methodology, Software, Resources. **Prashant K. Sharma**: Project administration, Conceptualization, Supervision, Methodology, Writing – review & editing.

Declaration of competing interest

The authors declare that they have no known competing financial interests or personal relationships that could have appeared to influence the work reported in this paper.

Acknowledgments

The UMT-3 tribometer (Bruker) setup was purchased thanks to the grant no. 91112026 from the Netherlands Organization for Health Research and Development (ZonMW). Graphic abstract and **Fig. 9** were created with BioRender.com. We also would like to thank the Sichuan International Science and technology Innovation Cooperation Project（2022YFH0062）for the support and China Scholarship Council for a 4-year scholarship to Drs. K. Ren (project no. CSC201806400039) and Drs. H. Wan (project no. CSC201606320244) to pursue their Ph.D.

References

1. Seror, J. *et al.* Articular cartilage proteoglycans as boundary lubricants: Structure and frictional interaction of surface-attached hyaluronan and hyaluronan-aggrecan complexes. *Biomacromolecules* **12**, 3432–3443 (2011).
2. Morgese, G., Cavalli, E., Mü, M., Zenobi-Wong, M. & Benetti, E. M. Nanoassemblies of Tissue-Reactive, Polyoxazoline Graft-Copolymers Restore the Lubrication Properties of Degraded Cartilage. *ACS Nano* **11**, 24 (2017).
3. Lin, W. & Klein, J. Recent Progress in Cartilage Lubrication. *Adv. Mater.* **2005513**, 1–23 (2021).
4. Jahn, S., Seror, J. & Klein, J. Lubrication of Articular Cartilage. *Annu. Rev. Biomed. Eng.* **18**, 235–258 (2016).
5. Gleghorn, J. P. & Bonassar, L. J. Lubrication mode analysis of articular cartilage using Stribeck surfaces. *J. Biomech.* **41**, 1910–1918 (2008).
6. Moore, A. C. & Burris, D. L. Tribological rehydration of cartilage and its potential role in preserving joint health. *Osteoarthr. Cartil.* **25**, 99–107 (2017).
7. Macconaill, M. A. The Function of Intra-Articular Fibrocartilages, with Special Reference to the Knee and Inferior Radio-Ulnar Joints. *J. Anat.* **66**, 210–27 (1932).
8. McCutchen, C. W. The frictional properties of animal joints. *Wear* **5**, 1–17 (1962).
9. Katta, J., Jin, Z., Ingham, E. & Fisher, J. Biotribology of articular cartilage-A review of the recent advances. *Med. Eng. Phys.* **30**, 1349–1363 (2008).
10. Seror, J. *et al.* Normal and shear interactions between hyaluronan-aggrecan complexes mimicking possible boundary lubricants in articular cartilage in synovial joints. *Biomacromolecules* **13**, 3823–3832 (2012).
11. Schmidt, T. A., Gastelum, N. S., Nguyen, Q. T., Schumacher, B. L. & Sah, R. L. Boundary lubrication of articular cartilage: role of synovial fluid constituents. *Arthritis Rheum.* **56**, 882–891 (2007).
12. Bonnevie, E. D., Galesso, D., Secchieri, C., Cohen, I. & Bonassar, L. J. Elastoviscous transitions of articular cartilage reveal a mechanism of synergy between lubricin and hyaluronic acid. *PLoS One* **10**, 1–15 (2015).
13. Greene, G. W. *et al.* Adaptive mechanically controlled lubrication mechanism found in articular joints. *Proc. Natl. Acad. Sci. U. S. A.* **108**, 5255–9 (2011).
14. Santavirta, S. Biotribology. *Acta Orthop.* **76**, 613 (2005).
15. Bonnevie, E. D., Galesso, D., Secchieri, C. & Bonassar, L. J. Degradation alters the lubrication of articular cartilage by high viscosity, hyaluronic acid-based lubricants. *J. Orthop. Res.* **36**, 1456–1464 (2018).

16. Mabuchi, K., Obara, T., Ikegami, K., Yamaguchi, T. & Kanayama, T. Molecular weight independence of the effect of additive hyaluronic acid on the lubricating characteristics in synovial joints with experimental deterioration. *Clin. Biomech.* **14**, 352–356 (1999).
17. Mori, S., Naito, M. & Moriyama, S. Highly viscous sodium hyaluronate and joint lubrication. *Int. Orthop.* **26**, 116–121 (2002).
18. Poole, A. R. *et al.* Type II collagen degradation and its regulation in articular cartilage in osteoarthritis. *Ann. Rheum. Dis.* **61**, 78–81 (2002).
19. Chu, C. R., Izzo, N. J., Irrgang, J. J., Ferretti, M. & Studer, R. K. Clinical diagnosis of potentially treatable early articular cartilage degeneration using optical coherence tomography. *J. Biomed. Opt.* **12**, 051703 (2007).
20. Forsey, R. W. *et al.* The effect of hyaluronic acid and phospholipid based lubricants on friction within a human cartilage damage model. *Biomaterials* **27**, 4581–4590 (2006).
21. Brandt, K. D. *et al.* Efficacy and safety of intraarticular sodium hyaluronate in knee osteoarthritis. ORTHOVISC Study Group. *Clin. Orthop. Relat. Res.* 130–43 (2001).
22. Neustadt, D., Caldwell, J., Bell, M., Wade, J. & Gimbel, J. Clinical effects of intraarticular injection of high molecular weight hyaluronan (Orthovisc) in osteoarthritis of the knee: a randomized, controlled, multicenter trial. *J. Rheumatol.* **32**, 1928–36 (2005).
23. Bellamy, N. *et al.* Viscosupplementation for the treatment of osteoarthritis of the knee. *Cochrane Database of Systematic Reviews* **2006**, (2006).
24. Campbell, K. A. *et al.* Is Local Viscosupplementation Injection Clinically Superior to Other Therapies in the Treatment of Osteoarthritis of the Knee: A Systematic Review of Overlapping Meta-analyses. *Arthrosc. J. Arthrosc. Relat. Surg.* **31**, 2036-2045.e14 (2015).
25. Maheu, E., Rannou, F. & Reginster, J.-Y. Efficacy and safety of hyaluronic acid in the management of osteoarthritis: Evidence from real-life setting trials and surveys. *Semin. Arthritis Rheum.* **45**, S28–S33 (2016).
26. Cook, S. G. & Bonassar, L. J. Interaction with Cartilage Increases the Viscosity of Hyaluronic Acid Solutions. *ACS Biomater. Sci. Eng.* **6**, 2787–2795 (2020).
27. Singh, A. *et al.* Enhanced lubrication on tissue and biomaterial surfaces through peptide-mediated binding of hyaluronic acid. *Nat. Mater.* **13**, 988–995 (2014).
28. Tadmor, R., Chen, N. & Israelachvili, J. N. Thin film rheology and lubricity of hyaluronic acid solutions at a normal physiological concentration. *J. Biomed. Mater. Res.* **61**, 514–523 (2002).

29. Neto, A. I., Vasconcelos, N. L., Oliveira, S. M., Ruiz-Molina, D. & Mano, J. F. High-Throughput Topographic, Mechanical, and Biological Screening of Multilayer Films Containing Mussel-Inspired Biopolymers. *Adv. Funct. Mater.* **26**, 2745–2755 (2016).
30. Neto, A. I. *et al.* Nanostructured polymeric coatings based on chitosan and dopamine-modified hyaluronic acid for biomedical applications. *Small* **10**, 2459–2469 (2014).
31. Zhou, D. *et al.* Dopamine-Modified Hyaluronic Acid Hydrogel Adhesives with Fast-Forming and High Tissue Adhesion. *ACS Appl. Mater. Interfaces* **12**, 18225–18234 (2020).
32. Kim, S. *et al.* Electrochemical deposition of dopamine-hyaluronic acid conjugates for anti-biofouling bioelectrodes. *J. Mater. Chem. B* **5**, 4507–4513 (2017).
33. Li, X. *et al.* Dopamine-functionalized hyaluronic acid microspheres for effective capture of CD44-overexpressing circulating tumor cells. *Colloids Surfaces B Biointerfaces* **196**, 111281 (2020).
34. Yang, M. *et al.* Selenium and dopamine-crosslinked hyaluronic acid hydrogel for chemophotothermal cancer therapy. *J. Control. Release* **324**, 750–764 (2020).
35. Wu, F. *et al.* Multifunctional Coating Based on Hyaluronic Acid and Dopamine Conjugate for Potential Application on Surface Modification of Cardiovascular Implanted Devices. *ACS Appl. Mater. Interfaces* **8**, 109–121 (2016).
36. Hong, S. *et al.* Hyaluronic acid catechol: A biopolymer exhibiting a pH-dependent adhesive or cohesive property for human neural stem cell engineering. *Adv. Funct. Mater.* **23**, 1774–1780 (2013).
37. Höök, F., Rodahl, M., Brzezinski, P. & Kasemo, B. Energy dissipation kinetics for protein and antibody−antigen adsorption under shear oscillation on a quartz crystal microbalance. *Langmuir* **14**, 729–734 (1998).
38. Majd, S. E. *et al.* Both hyaluronan and collagen type II keep proteoglycan 4 (lubricin) at the cartilage surface in a condition that provides low friction during boundary lubrication. *Langmuir* **30**, 14566–14572 (2014).
39. Kuijer, R., Van De Stadt, R. J., De Koning, M. H. M. T. & Van Der Korst, J. K. Influence of Constituents of Proteoglycans on Type II Collagen Fibrillogenesis. *Coll. Relat. Res.* **5**, 379–391 (1985).
40. Majd, S. E. *et al.* An in vitro study of cartilage–meniscus tribology to understand the changes caused by a meniscus implant. *Colloids Surfaces B Biointerfaces* **155**, 294–303 (2017).
41. Chan, S. M. T., Neu, C. P., DuRaine, G., Komvopoulos, K. & Reddi, A. H. Atomic

force microscope investigation of the boundary-lubricant layer in articular cartilage. *Osteoarthr. Cartil.* **18**, 956–963 (2010).
42. Lee, H. *et al.* Substrate-independent layer-by-layer assembly by using mussel-adhesive- inspired polymers. *Adv. Mater.* **20**, 1619–1623 (2008).
43. Xu, W. *et al.* Hyaluronic Acid-Functionalized Gold Nanorods with pH/NIR Dual-Responsive Drug Release for Synergetic Targeted Photothermal Chemotherapy of Breast Cancer. *ACS Appl. Mater. Interfaces* **9**, 36533–36547 (2017).
44. Kim, K., Kim, K., Ryu, J. H. & Lee, H. Chitosan-catechol: A polymer with long-lasting mucoadhesive properties. *Biomaterials* **52**, 161–170 (2015).
45. Singh, A., Zhan, J., Ye, Z. & Elisseeff, J. H. Modular multifunctional poly(ethylene glycol) hydrogels for stem cell differentiation. *Adv. Funct. Mater.* **23**, 575–582 (2013).
46. Mazzucco, D., McKinley, G., Scott, R. D. & Spector, M. Rheology of joint fluid in total knee arthroplasty patients. *J. Orthop. Res.* **20**, 1157–1163 (2002).
47. Wan, H., Zhao, X., Lin, C., Kaper, H. J. & Sharma, P. K. Nanostructured Coating for Biomaterial Lubrication through Biomacromolecular Recruitment. *ACS Appl. Mater. Interfaces* **12**, 23726–23736 (2020).
48. LEWIS, P. R. & McCUTCHEN, C. W. Mechanism of Animal Joints: Experimental Evidence for Weeping Lubrication in Mammalian Joints. *Nature* **184**, 1285 (1959).
49. Caligaris, M. & Ateshian, G. A. Effects of sustained interstitial fluid pressurization under migrating contact area, and boundary lubrication by synovial fluid, on cartilage friction. *Osteoarthr. Cartil.* **16**, 1220–1227 (2008).
50. Pawaskar, S. S., Jin, Z. M. & Fisher, J. Modelling of fluid support inside articular cartilage during sliding. *Proc. Inst. Mech. Eng. Part J J. Eng. Tribol.* **221**, 165–174 (2007).
51. Chan, S. M. T., Neu, C. P., Komvopoulos, K. & Reddi, A. H. The role of lubricant entrapment at biological interfaces: Reduction of friction and adhesion in articular cartilage. *J. Biomech.* **44**, 2015–2020 (2011).
52. Wan, H., Ren, K., Kaper, H. J. & Sharma, P. K. A bioinspired mucoadhesive restores lubrication of degraded cartilage through reestablishment of lamina splendens. *Colloids Surfaces B Biointerfaces* **193**, 110977 (2020).
53. Katta, J., Pawaskar, S. S., Jin, Z. M., Ingham, E. & Fisher, J. Effect of load variation on the friction properties of articular cartilage. *Proc. Inst. Mech. Eng. Part J J. Eng. Tribol.* **221**, 175–181 (2007).
54. Soltz, M. A. & Ateshian, G. A. Experimental verification and theoretical prediction of cartilage interstitial fluid pressurization at an impermeable contact interface in

confined compression. *J. Biomech.* **31**, 927–934 (1998).
55. Ateshian, G. A. *et al.* The role of osmotic pressure and tension-compression nonlinearity in the frictional response of articular cartilage. *Transp. Porous Media* **50**, 5–33 (2003).
56. Nedomová, B., Budáčová, J., Frištáková, M. & Šagát, T. Contributions of Muscles, Ligaments, and the Ground-Reaction Force to Tibiofemoral Joint Loading During Normal Gait. *Lek. Obz.* **65**, 354–359 (2016).
57. Abubacker, S., McPeak, A., Dorosz, S. G., Egberts, P. & Schmidt, T. A. Effect of counterface on cartilage boundary lubricating ability by proteoglycan 4 and hyaluronan: Cartilage-glass versus cartilage–cartilage. *J. Orthop. Res.* **36**, (2018).

Supporting information

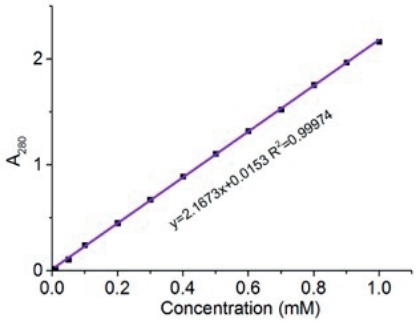

Fig. S1 Uv-Vis spectra of dopamine solution at A280 with concentrations ranging from 0.1 mM to 1 mM; the standard curve was calculated by linear fitting.